Supporting Information

Structural-Energetic Basis for Coupling between Equilibrium Fluctuations and Phosphorylation in a Protein Native Ensemble

Hemashree Golla[1], Adithi Kannan[1], Soundhararajan Gopi[1], Sowmiya Murugan[1],

*Lakshmi R Perumalsamy[2] & Athi N. Naganathan[1]**

[1]Department of Biotechnology, Bhupat & Jyoti Mehta School of Biosciences, Indian Institute of Technology Madras, Chennai 600036, India.

[2]Department of Biomedical Sciences, Sri Ramachandra Institute of Higher Education and Research, Chennai 600116, India.

*e-mail: athi@iitm.ac.in

Supporting Information Text

p190A RhoGAP FF1 Gene Sequence (FF1)

5'ATGAGCCAGCAAATCGCGACCGCGAAGGACAAATACGAGTGGCTGGTGAGCCGT
ATTGTTAAGAACCACAACGAAAACTGGCTGAGCGTGAGCCGTAAAATGCAGGCGAG
CCCGGAGTATCAAGATTACGTTTATCTGGAAGGCACCCAGAAGGCGAAGAAACTGT
TCCTGCAACACATCCACCGTCTGAAACACGAGCACATTGAACGT **3'**

Primers Used

Protein	Primer Sequence
WT	5' CAAATACGAGtttCTGGTGAGCCGTATTG 3' 5' TCCTTCGCGGTCGCGATT 3'
K53E	5' GAAGGCGAAGgagCTGTTCCTGC 3' 5' TGGGTGCCCTCCAGATAC 3'
K53Q	5' GAAGGCGAAGcaaCTGTTCCTGC 3' 5' TGGGTGCCCTCCAGATAC 3'
W13E	5'CAAATACGAGgagCTGGTGAGCCGTATTG 3' 5'TCCTTCGCGGTCGCGATT 3'

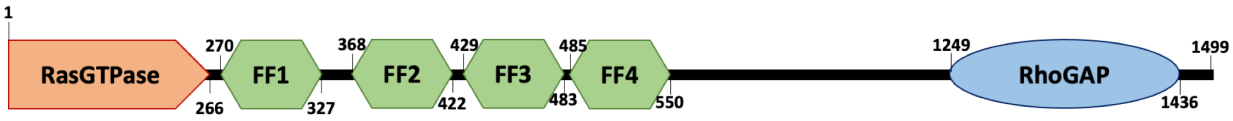

Figure S1 Domain architecture of human p190A Rho GTPase-activating protein (RhoGAP; Uniprot Q9NRY4).

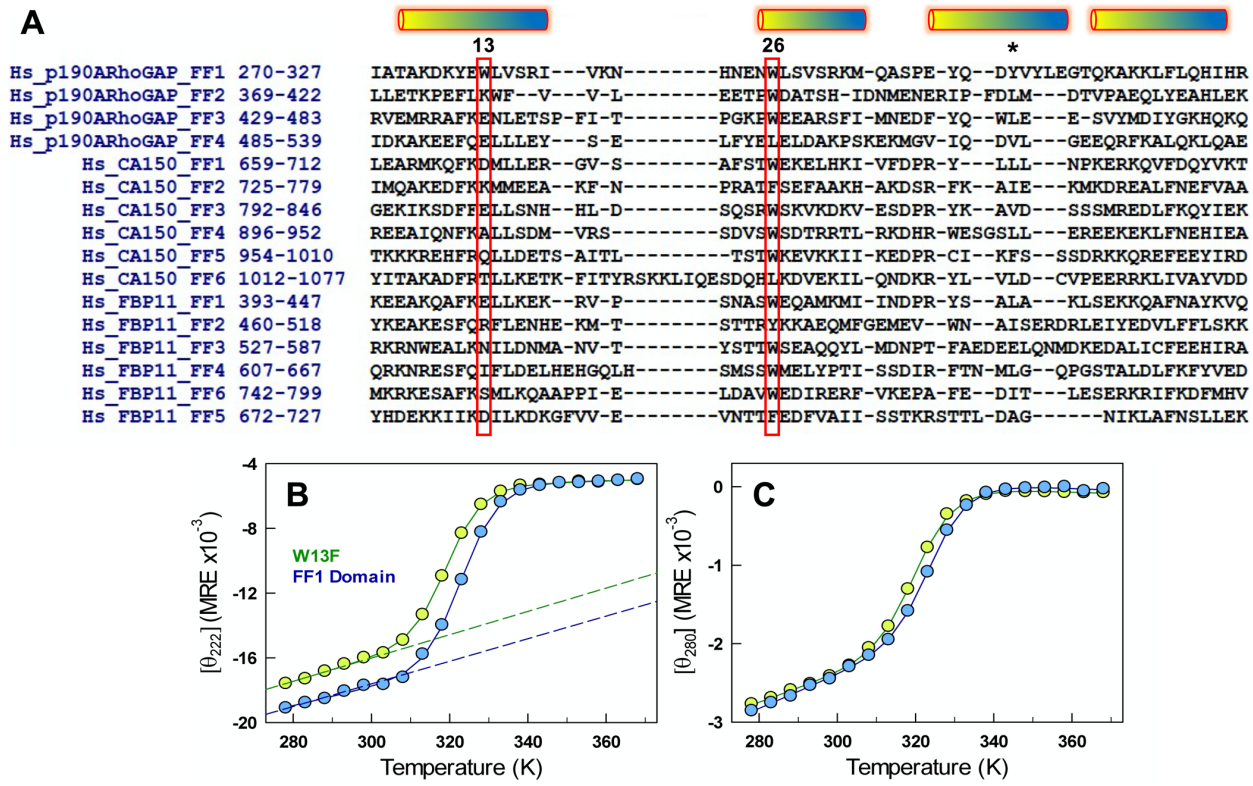

Figure S2 (A) Multiple sequence alignment of FF domains from p190-A Rho-GAP, CA150, and FBP11 proteins. Position 13 is variable, while position 26 is highly conserved (red boxes). The symbol * signals the phosphorylated tyrosine. The cartoon on top marks the helix boundaries with respect to the p190A RhoGAP FF1 domain (first sequence). (B and C) Thermal unfolding curves of FF1 domain (blue) and W13F variant (green; labeled as WT in the main text) as monitored by far-UV CD at 222 nm (panel B) and near-UV CD at 280 nm (panel C).

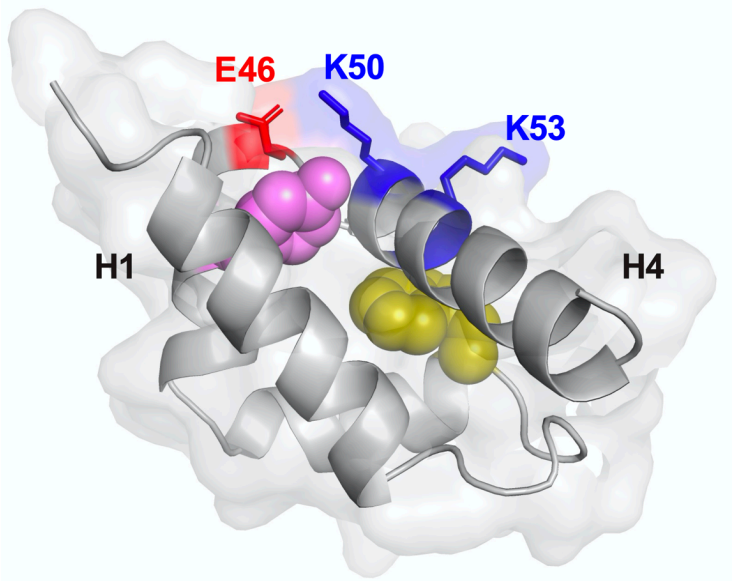

Figure S3 Structure of the FF1 domain highlighting the interaction of K50 with E46 that ensures the net stabilization free-energy of K50 is favorable. Y42 and W26 are shown in magenta and olive green, respectively. H1 and H4 stand for helices 1 and 4, respectively.

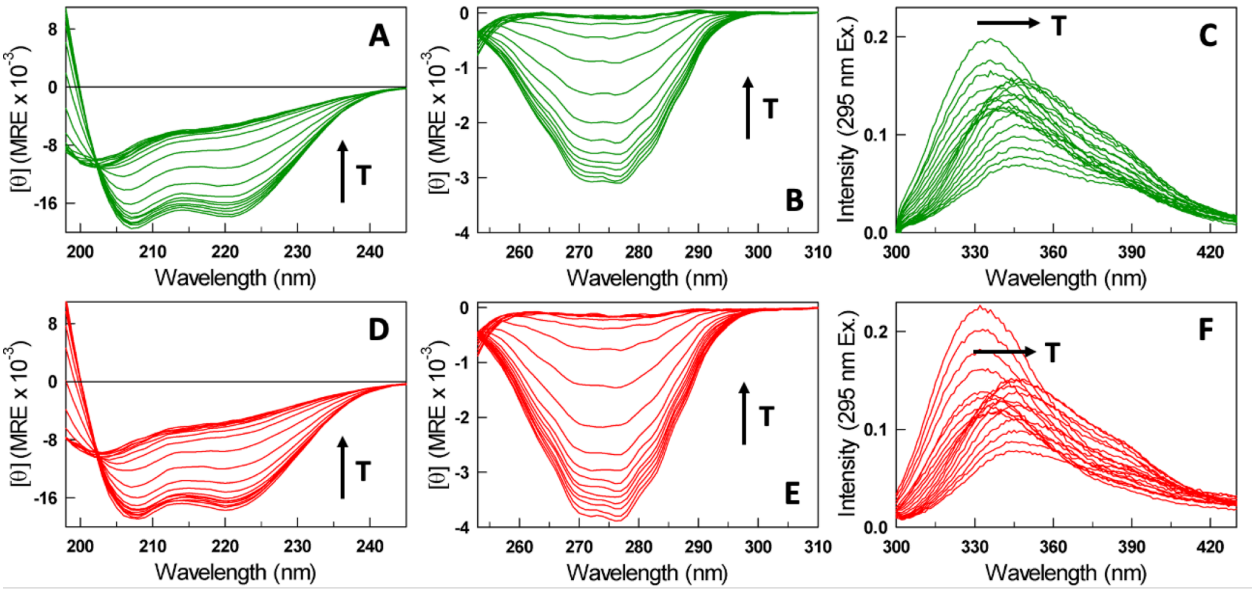

Figure S4 Far-UV CD spectra (left column), near-UV CD spectra (middle column), and fluorescence emission spectra (295 nm excitation) of the WT (top row) and K53E mutant (bottom row), respectively. Arrows point in the direction of increasing temperature T. In fluorescence, the emission intensity decreases apart from shifts in the emission maxima.

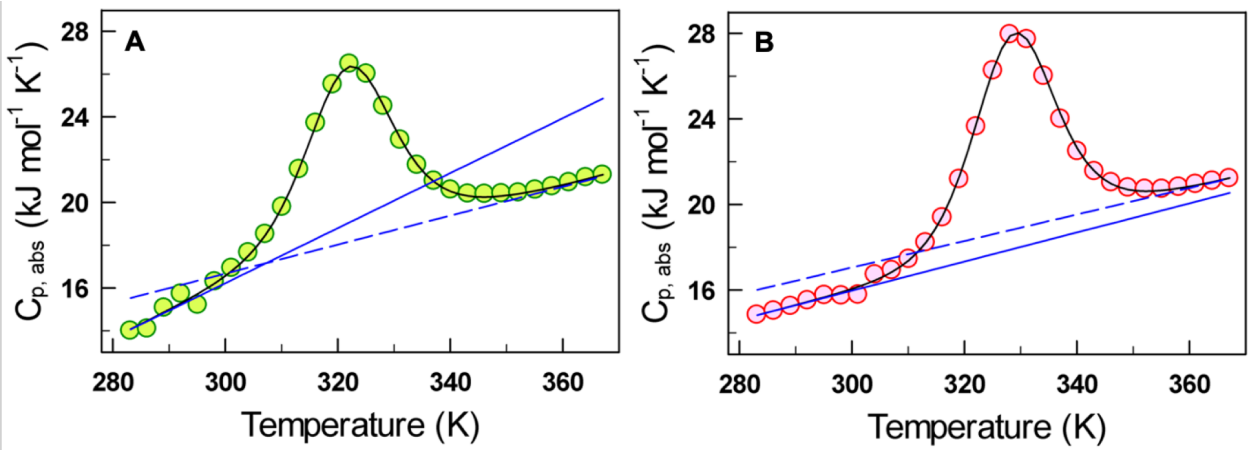

Figure S5 Two-state model fits (black curves) to the DSC curves of the WT (panel A) and K53E (panel B). Note the unphysical crossing folded (continuous blue) and unfolded baselines (dashed blue) for the WT, while the baselines are near-parallel for the K53E mutant.

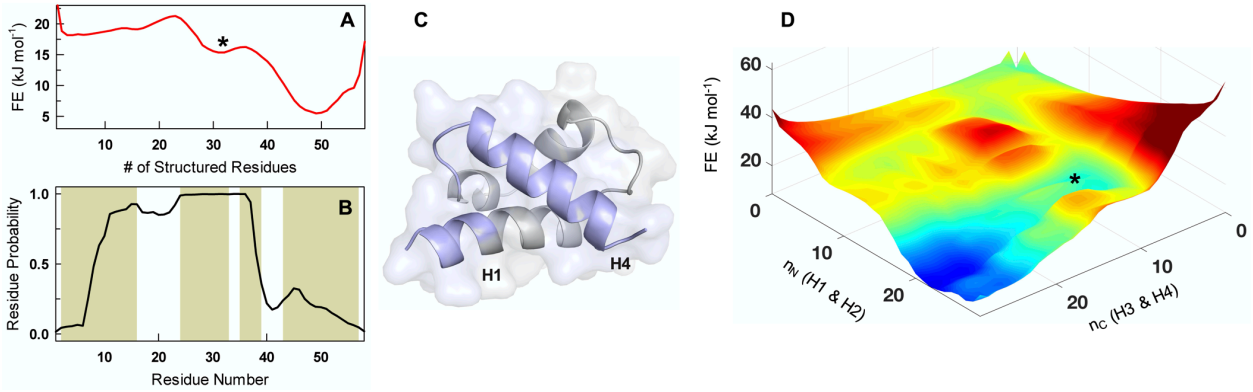

Figure S6 Panel A represents the WSME-model derived free-energy profile of the HYPA/FBP11 FF domain at 310 K, employing identical parameters to the one used for the WT FF1 domain (green in Figure 3A in the main text). The asterisk (*) on the free-energy profile represents an intermediate state whose residue folding probability is shown in panel B and structure in panel C (blue represents disordered regions). Panel D is the two-dimensional free-energy landscape with the position of the intermediate marked with an asterisk.

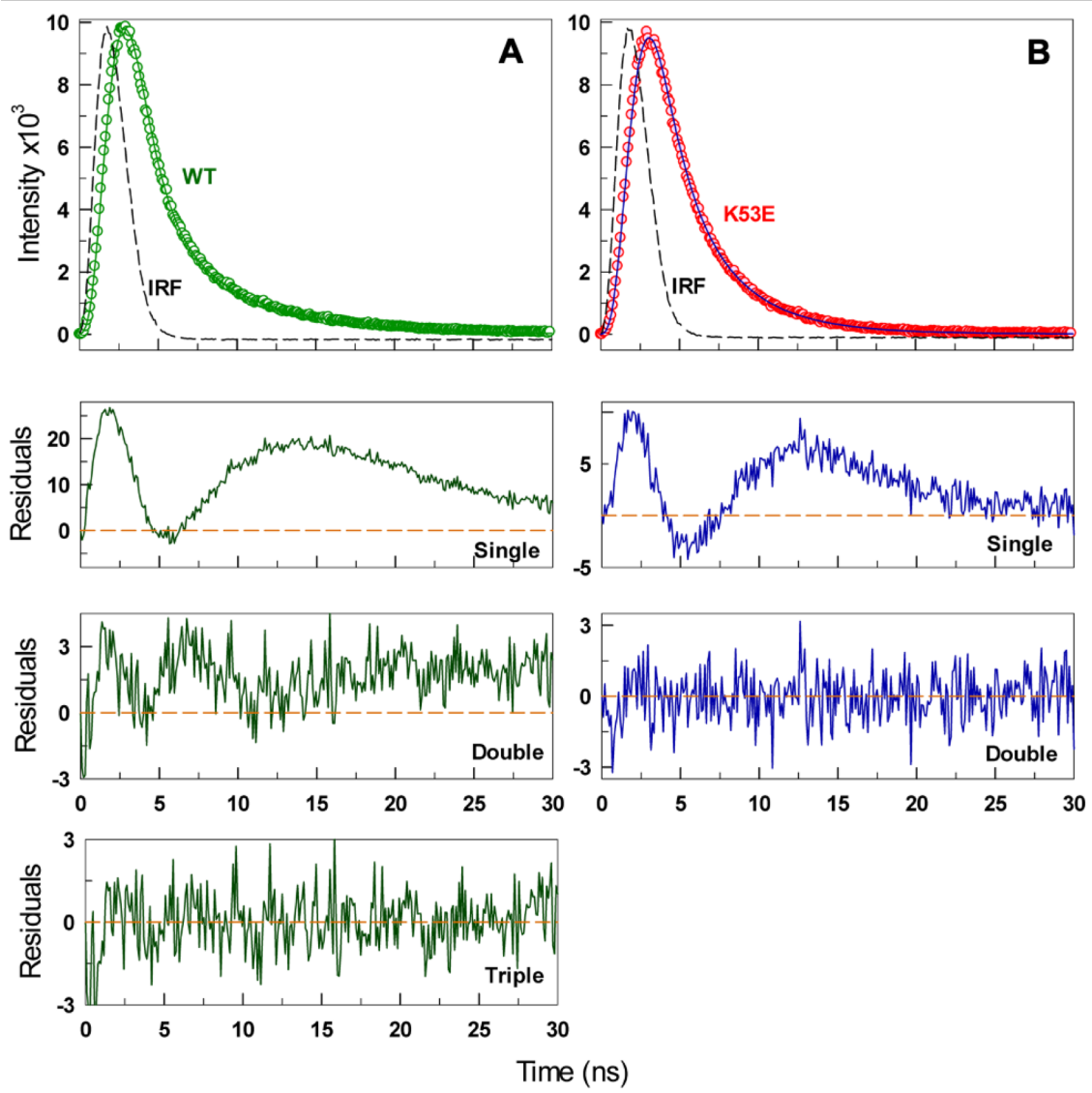

Figure S7 Fluorescence intensity transients of the WT and K53E at 298 K. The residuals from fits to different components – single-, bi- and tr-exponentials – are shown below the primary panels A and B. Note that a bi-exponential fit is sufficient to fully account for the shape of the transient for the K53E variant, while the residuals average to zero for the WT only for a tri-exponential fit. IRF is the instrument response function.

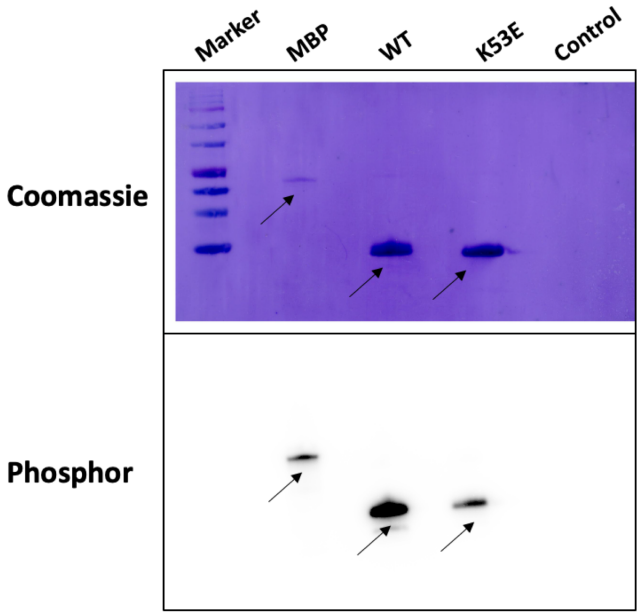

Figure S8 Representative phosphor images and Coomassie-stained membranes at 310 K. Myelin basic protein (MBP) is used as a positive control while the lane marked 'Control' is the negative control in which substrate proteins are not added.

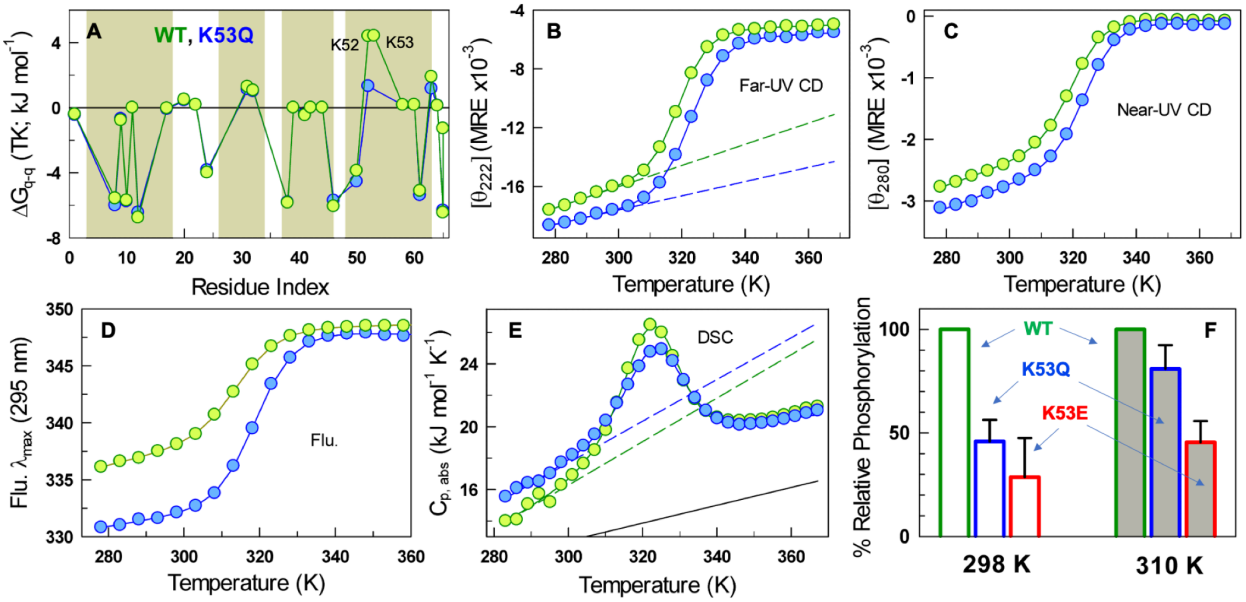

Figure S9 (A) Tanford-Kirkwood electrostatic free energy calculations highlighting that K53Q mutant should exhibit no electrostatic frustration at position 53 (as glutamine is a neutrally charged). Eliminating the unfavorable interaction at position 53, therefore, reduces the frustration for the residue K52 as well. (B) Far-UV CD unfolding curves of the WT (green) and the mutant K53Q (blue) at 222 nm. The dashed lines represent the pre-transition baselines. Note that the pre-transition baseline slopes are higher for the WT but smaller for the K53Q mutant despite exhibiting little changes in stability (T_m of ~320 K for the WT and ~323 K for K53Q). (C) Near-UV CD monitored thermal melts of the WT and K53Q at 280 nm. Here, the K53Q mutant has a more compact native ensemble similar to K53E, but the differences are smaller (compare with Figure 2C in the main text). (D) Fluorescence emission maximum of W26 (on excitation at 295 nm) for the WT and K53Q mutant. Note that the mutant has a substantially blue-shifted emission maximum, similar to that of the K53E mutant. (E) Both the WT and the K53Q mutant exhibit broad pre-transition baselines from DSC, though the pre-transition slope is marginally weaker for the latter. (F) Since the K53Q mutant exhibits properties in between that of the WT and the K53E mutant, one expects the phosphorylation extents to follow the same trend. True to this, we observe that though the K53Q mutation suppresses phosphorylation (in comparison with the WT), it does not do so to the same extent as the K53E mutation.

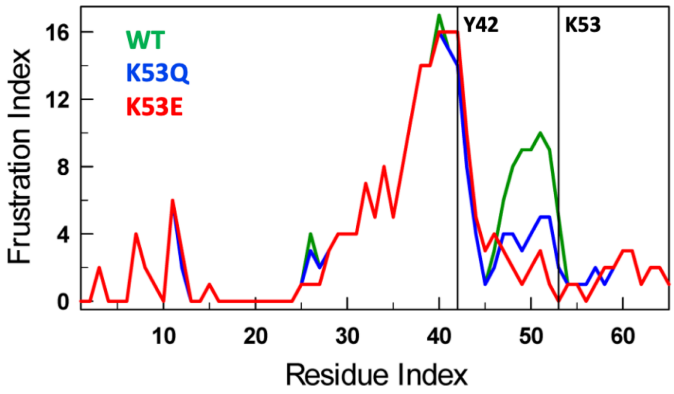

Figure S10 Highly frustrated residues in the FF1 domain variants as predicted by the Frustratometer web-server (http://frustratometer.qb.fcen.uba.ar/).

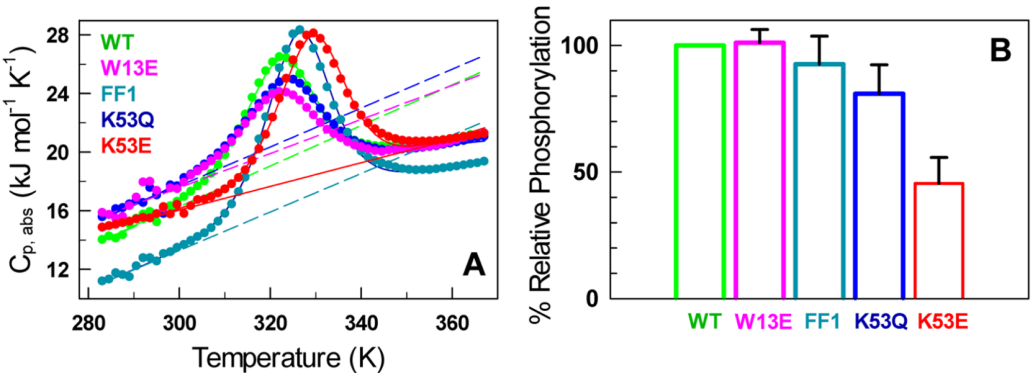

Figure S11 Control experiments with variants FF1 (with W at position 13 as in the original FF1 sequence) and W13E. (A) All heat capacity profiles display similar pre-transition slopes (dashed lines), except for K53E, which is noticeably flatter (continuous red line) and indicative of lower enthalpic fluctuations. (B) Percentage relative phosphorylation of the different variants at 310 K.